Resonances in photoionization: Cross sections for vibrationally excited H_2

J. Zs. Mezei,[1,2,*] I. F. Schneider,[1,†] E. Roueff,[3] and Ch. Jungen[2,‡]

[1]*Laboratoire Ondes et Milieux Complexes UMR-6294 CNRS et Université du Havre, 25, rue Philippe Lebon, BP 540, 76058 Le Havre, France*

[2]*Laboratoire Aimé Cotton du CNRS, Bâtiment 505, Université de Paris-Sud, F-91405 Orsay, France*

[3]*LUTH, Observatoire de Paris et Université Paris 7, F-92190 Meudon, France*

(Received 27 January 2012; published 13 April 2012)

Multichannel quantum defect theory is used to calculate photoionization cross sections for vibrationally excited diatomic hydrogen. The calculations are based on the state-of-the-art clamped-nuclei potential energy curves and electronic dipole transition moments of Wolniewicz. The calculations indicate that, in contrast to what had been assumed previously, autoionization resonances dominate the cross section.

DOI: 10.1103/PhysRevA.85.043411 PACS number(s): 33.80.Eh, 33.20.Wr, 33.50.Dq, 33.80.Gj

I. INTRODUCTION

Diatomic molecular hydrogen is the most abundant molecule in interstellar molecular clouds [1]. The modeling [2] of these environments relies on accurate cross sections for the various relevant processes. Among them, photoionization plays a major role in the kinetics and in the energy exchanges involving H_2. The recent discovery of vibrationally excited molecular hydrogen in extragalactic environments [3] and toward HD37903 [4,5] suggests that photoionization of molecular hydrogen arising from vibrationally excited levels by photons of 13.6 eV or less is possible and should be introduced in the modeling of interstellar photon dominated regions.

The only comprehensive experimental and theoretical results concerning bound-bound radiative processes in H_2 are currently available in the MOLAT database [6], where the relevant R, Q, and P transition energies involving vibrationally excited levels are listed. Abgrall *et al.* [7–10] provided theoretical spontaneous emission probabilities for these transitions. The MOLAT database is limited to excited electronic states with $n \leqslant 3$ (B, C, B', and D states), which are the only ones accessible below the Lyman cutoff when excitation from the vibrational ground level of H_2 is considered. However, excitation, for instance, from $v'' = 4$ with radiation $\lambda \geqslant 91$ nm populates the full Rydberg manifold of H_2 and leads to photoionization as well.

Only a limited amount of theoretical work on photoionization from vibrationally excited molecular hydrogen has been carried out. In 1975 Ford, Docken, and Dalgarno [11,12] published photoionization cross sections based on a correlated initial-state electronic wave function, while employing simple one-center hydrogen atom Coulomb functions for the continuum final state. In 1977 Flannery, Tai, and Albritton [13] published extensive tables of vibrationally resolved photoionization cross sections in which the initial state was described in a more primitive manner than in Ref. [11], but where a more realistic two-center representation was used for the continuum wave function of the final state. A more elaborate calculation was published in 1978 by ONeil and Reinhardt [14] who used correlated wave functions for both the initial and the final state. In all these calculations bound-to-continuum electronic dipole transition moments were employed, evaluated as functions of the internuclear distance. The calculations of Refs. [11–14] all predict the background photoionization cross section (direct ionization), but none of them takes account of resonant (autoionizing) structures. These early results are still used by the astrophysical community when photoionization needs to be included in the kinetic models. This is the case, for instance, in the very recent paper by Coppola *et al.* [15] on the vibrationally resolved kinetics for molecular hydrogen and its cation in the primordial universe chemistry.

In the present paper we address the topic of calculating photoionization cross sections for excitation from excited vibrational levels of the ground state. Our calculations are based on multichannel quantum defect theory (MQDT) which allows us to take account of the full manifold of Rydberg states and their interactions with the electronic continuum. We show that the photoionization cross section is actually dominated by resonance effects, in the sense that autoionizing resonances produce a major fraction of the averaged cross section. We exemplify this here by focusing on the particular case of the $Q(1)$ transitions ($\Delta N = 0$, N total molecular angular momentum exclusive of spins) originating from the $v'' = 1, N'' = 1$ ground-state level. The main conclusions, however, which we reach here, remain valid also for excitation from other v'', N'' initial levels. Indeed, the theoretical photoabsorption and photoionization spectra displayed in Fig. 1 below for $v'' = 1$ and 5 demonstrate the generic character of those plots, in that for $v'' \neq 1$ the same spectral structures occur, albeit with different intensities and a shifted abscissa scale. Analogous results dealing with the P and R optical dipole transitions ($\Delta N = -1$ and $+1$, respectively) will be published subsequently, and a detailed compilation of the transition energies, Einstein A coefficients as well as photoionization cross sections for various v'', N'' values will also be published later [16].

II. THEORETICAL APPROACH

A. Background

Absorption transitions to the $3p\pi\, D\, ^1\Pi_u$ state of the H_2 molecule have recently been reinvestigated with different techniques on two synchrotron installations. Absolute absorption cross sections have been obtained with the 10-m normal

[*]Also at Institute of Nuclear Research of the Hungarian Academy of Science, P. O. Box 51, H-4001 Debrecen, Hungary.

[†]Work performed partly in visit at the Laboratoire Aimé Cotton, Orsay, France.

[‡]Also at Department of Physics and Astronomy, University College London, London WC1E 6BT, United Kingdom.

 ©2012 American Physical Society

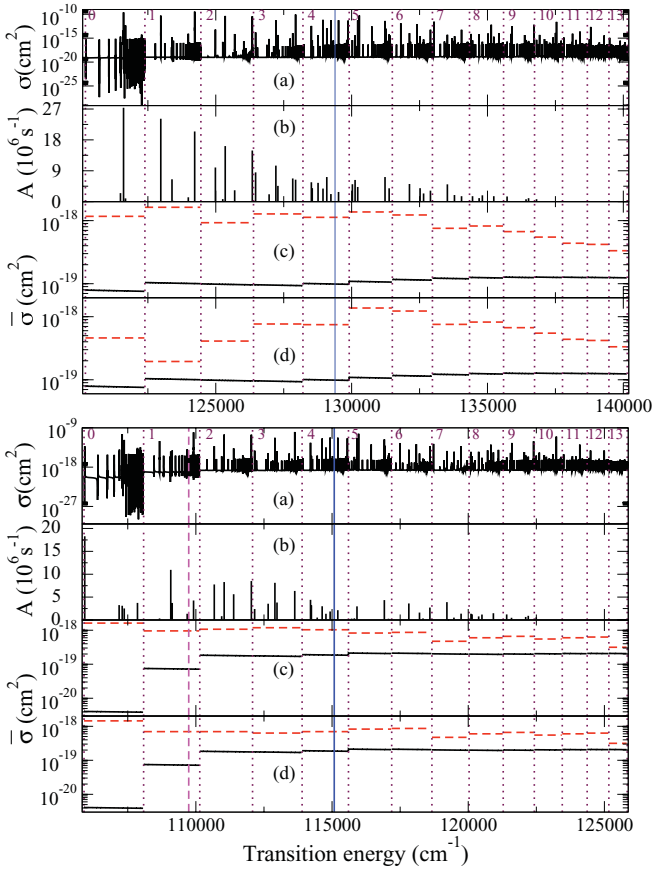

FIG. 1. (Color online) Upper frame: cross sections and line intensities for the $Q(1)$ transitions from the $X\,^1\Sigma_g^+$, $v'' = 1$ ground state of the H_2 molecule. The vertical dotted lines represent the vibrational ionization thresholds, starting with $v^+ = 0$ and ending with $v^+ = 14$. The vertical continuous line (blue online) indicates the position of the H + H ($n = 3$) dissociation limit of H_2. (a) Continuum photoabsorption cross section. (b) Spontaneous emission coefficients for the transitions listed in Table I, equivalent to the resonant part ($n = 3$–6) of the cross section. (c) Photoabsorption. Continuous black lines: background cross section $\sigma^{(\text{background})}(E)$. Dashed lines (red online): averaged full cross section. (d) Photoionization. [Same symbols as in (c).] Lower frame: the same for $v'' = 5$. The dashed vertical line (magenta online) indicates the energy corresponding to the Lyman cutoff.

incidence scanning monochromator at the BESSY II synchrotron (Berlin) [17]. These results were exploited by Glass-Maujean and co-workers [18–20] to obtain quantitative information on competing ionization, dissociation, and intramolecular fluorescence decay for the $D\,^1\Pi_u$ vibrational series. The positions and absolute intensities of the higher $np\pi\,^1\Pi_u^-$ ($n = 2$–30) $\leftarrow X\,^1\Sigma_g^+, v'' = 0$ $Q(N)$ ($N = 1$–4) absorption transitions of H_2 were also obtained and interpreted with the help of MQDT calculations. Quite recently the Fourier transform spectrometer operating in the vacuum ultraviolet wavelength range of the DESIRS beamline at the SOLEIL synchrotron (Saclay, France) has been used for recording absorption spectra and measure line positions and profiles with significantly increased spectral resolution [21].

These papers demonstrated that the new synchrotron frequency measurements approach the accuracy of the best traditional spectrographic measurements which are known to be better than a fraction of a wave number unit. All the published new experimental data turn out to be in very good agreement with the *ab initio* multichannel quantum defect theory (MQDT) calculations, both with regard to transition frequencies, absolute line intensities, and the competition between the various decay processes. In particular the MQDT calculations provide energy-level positions which are globally correct to better than $\approx 1\ \text{cm}^{-1}$.

Building on this earlier work [18–20] we study here the photoexcitation of vibrationally excited H_2. We compute energy levels, wave functions, spontaneous emission Einstein coefficients, and photoionization cross sections using the same MQDT techniques [22–24] and the same input parameters used in the preceding papers [18–20]. This approach guarantees that the computed cross sections will be of the same quality as obtained before for $v'' = 0$, despite the fact that for $v'' > 0$ much less experimental information for comparison and checks is available. In particular, no absolute intensity measurements exist for $v'' > 0$. In the following we briefly review the main procedures and steps of the computations. Standard (SI) units are used throughout, except when explicitly stated otherwise.

B. Multichannel quantum defect theory

The manifold of $^1\Pi_u$ excited states of H_2 is assumed to represent a single unperturbed $np\pi$ Rydberg series converging to the $X\,^2\Sigma_g^+$ ground state of H_2^+. The quantum defects may thus be extracted directly from the clamped-nuclei (Born-Oppenheimer) potential energy curves (PEC) by use of the one-channel Rydberg equation, written here in atomic units as a geometry-dependent function:

$$U_n(R) = U^+(R) - \frac{1}{2\,[n - \mu_n(R)]^2}. \tag{1}$$

A comment concerning the validity of the single-channel–single-partial-wave approximation employed here appears necessary. Rydberg states of ungerade symmetry associated with the higher partial waves $f\pi$ and $h\pi$ have been identified by infrared Fourier transform spectroscopy years ago and their energies have been determined to high precision [25]. However, transitions to these states have never been identified in the absorption spectrum from the ground state despite repeated searches by one of the present authors (Ch.J.), nor have they been seen in excitation from the $2s\,EF\,^1\Sigma_g^+$ excited state [26], obviously because of the weakness of the corresponding electronic transitions. Indeed, the quantum-chemical dipole transition moment computations of Ref. [27] predict that for instance for $n = 4$ at equilibrium ($R = 1.4$ a.u.), the $X \rightarrow 4f\pi$ excitation cross section is 2.8×10^4 times weaker than $X \rightarrow 4p\pi$ and may therefore be safely neglected. The state-of-the-art excited potential energy curves [28] which we shall use below to determine the quantum defects functions that appear in Eq. (1), have been computed in a sophisticated scheme in which large numbers of optimized singly and doubly excited configurations are superposed which correspond to higher parent ion states than the $H_2^+\,^2\Sigma_g^+$ ground state which is taken into account explicitly in this work. Their contributions are absorbed here into the quantum defect functions which

therefore to some extent have an effective character. It is clear that this simplified approach is limited to energies not too far above the first electronic ionization threshold, and will eventually fail when high energies are considered, e.g., near the second electronic ionization threshold corresponding to H_2^+ $A\,^2\Sigma_u^+$. In such a situation more channels and their interactions must be included explicitly in the quantum defect treatment.

The index n of the quantum defect μ in Eq. (1) indicates that this quantity may vary slightly with the principal quantum number n, i.e., it is energy dependent. This energy dependence is formally parametrized as an expansion in terms of the electron binding energy ϵ (in a.u.):

$$\mu(\epsilon,R)=\mu^{(0)}(R)+\epsilon\mu^{(1)}(R)+\frac{1}{2}\epsilon^2\mu^{(2)}(R)+\frac{m}{M}\mu^{\rm spec}(R). \tag{2}$$

The three coefficients $\mu^{(k)}(R)$, $k=0,1,2$ that appear in Eq. (2) are determined by means of Eq. (1) from the three clamped nuclei PEC, $U_n(R)$, of the $np\pi$,$n=2,3,4$ Rydberg states computed by Wolniewicz and co-workers [27–29], combined with the PEC, $U^+(R)$, of the ion ground state $X\,^2\Sigma_g^+$ [30]. The clamped-nuclei electron binding energy is given for each R-value by the difference $\epsilon=\epsilon(R)=U_n(R)-U^+(R)$. $\mu^{\rm spec}(R)$ is related to the mass polarization term arising from the cross term $H_3'=-(m/4M)\nabla_1\nabla_2$ of the molecular Hamiltonian [31] (m electron mass, M nuclear reduced mass). $H_3'(R)$ has also been evaluated *ab initio* by Wolniewicz and co-workers [29].

The electronic dipole transition moments constitute a second set of input data required for the description of radiative electronic transitions. Energy-dependent clamped-nuclei electronic channel transition moments are parametrized in analogy with Eq. (2) as

$$d(\epsilon,R)=d^{(0)}(R)+\epsilon d^{(1)}(R)+\tfrac{1}{2}\epsilon^2 d^{(2)}(R). \tag{3}$$

These quantities are energy normalized and have the dimension (length) $\times$ (energy)$^{-1/2}$. The coefficients $d^{(q)}(R)$, $q=0,1,2$, may be derived directly from the *ab initio* clamped-nuclei dipole transition moments of Wolniewicz and co-workers [27,29]; see Ref. [18].

Upper state energy levels and/or continuum states and the rovibronic dipole transitions leading to them are computed using standard MQDT techniques [22–24]. The transition of the excited electron from the molecule-fixed reference frame to the space-fixed frame is described by a frame transformation which takes account of the nonadiabatic effects. In the case of the $Q(N)$ spectral lines corresponding to upper states of pure $^1\Pi_u^-$ symmetry there is no rotational nonadiabatic coupling so that, neglecting spin-orbit and hyperfine effects, the frame transformation reduces to evaluating integrals involving the initial- and final-state vibrational wave functions:

$$\mu^{(q,N,d)}_{v^+N^+,v^{+\prime}N^{+\prime}}=\int\chi_{v^+N^+}(R)\mu^{(q)}(R)\chi_{v^{+\prime}N^{+\prime}}(R)dR, \tag{4}$$

for the vibronic quantum defect, and

$$d^{(q,N,d)}_{v^+N^+,v''N''}=\int\chi_{v^+N^+}(R)d^{(q)}(R)\chi_{v''N''}(R)dR, \tag{5}$$

for the vibronic transition moments. Here $q=0,1,2$ as in Eqs. (2) and (3). The $Q(N)$ transitions studied here require that the total angular momenta of the molecule N',N'' and of the molecular ion $N^+,N^{+\prime}$ all be equal, i.e., $N=N^+=N^{+\prime}=N''$. d refers to the Kronig's symmetry label, designating levels that have total parity $-(-1)^N$.

The energy dependences of the vibronic quantum defects and dipole moment matrix elements of Eqs. (4) and (5) have the same functional form as those given in the Eqs. (2) and (3), with the difference that instead of ϵ one must use a vibrationally averaged value, $\bar{\epsilon}$. For the quantum defects the appropriate choice is $\bar{\epsilon}=\frac{1}{2}[(E-E^+_{v^+N^+})+(E-E^+_{v^{+\prime}N^{+\prime}})]$ [24], where E denotes the total energy and $E^+_{v^+N^+}$ are the vibration-rotation levels of the ion ground state. For the transition moments one chooses $\bar{\epsilon}=(E-E^+_{v^+N^+})$ [24]. Once the rovibronic quantum defects have been evaluated they must be converted into the so-called $\mathcal{S}$ and $\mathcal{C}$ matrices which are related to the reaction matrix $\mathbf{K}$ according to $\mathbf{K}=\mathcal{S}\mathcal{C}^{-1}$. This is achieved by means of procedures described in Refs. [32,33]. The "eigen-channel" formulation of MQDT [24] rewrites these matrices in the form $\mathcal{S}=\mathbf{U}\sin\pi\mu\mathbf{U}^{\rm T}$ and $\mathcal{C}=\mathbf{U}\cos\pi\mu\mathbf{U}^{\rm T}$, where $\mathbf{U}$ is the eigenvector matrix of the reaction matrix $\mathbf{K}$, while $\tan\pi\mu_\alpha$ are its eigenvalues and their arguments μ_α are the associated eigenquantum defects. [The indices α indicate that these quantities are not to be confused with the quantum defects that appear in Eqs. (2) and (4).]

Applying the asymptotic boundary conditions to the total wave function, one arrives at the generalized eigenvalue system [24]:

$$\mathbf{\Gamma B}=\tan\beta\mathbf{\Lambda B}, \tag{6}$$

where

$$\begin{aligned}
\Gamma_{ii'}&=\sin\beta_i\mathcal{C}_{ii'}+\cos\beta_i\mathcal{S}_{ii'},\quad i\in\text{closed}\\
\Lambda_{ii'}&=0,\quad i\in\text{closed}\\
\Gamma_{ii'}&=\mathcal{S}_{ii'},\quad i\in\text{open}\\
\Lambda_{ii'}&=\mathcal{C}_{ii'},\quad i\in\text{open}\\
\beta_i&=-\pi\nu_i,\quad i\in\text{closed}\\
\beta_i&=+\pi\tau_i,\quad i\in\text{open}.
\end{aligned} \tag{7}$$

If bound levels and discrete line intensities are to be evaluated (because there are no open channels or because open channels are neglected), Eq. (7) reduces to a homogenous set of linear equations, namely

$$\sum_k[\cos(\pi\nu_j)\mathcal{S}_{jk}+\sin(\pi\nu_j)\mathcal{C}_{jk}]B_k(E)=0, \tag{8}$$

where $\nu_j(E)=\sqrt{-\mathcal{R}hc/(E-E_j^+)}$ are the channel effective quantum numbers, B_k are the channel mixing coefficients, and $\mathcal{R}$ is the Rydberg constant. The indices j and k run over all vibrational channels v^+N^+ corresponding to the given N^+ value. By searching for zeros of Eq. (8) one finds the energies E_n of the bound levels and the corresponding channel mixing coefficients. The former, in wave number units and defined relative to the ionization thresholds, are

$$[(E_n-E^+_{v^+N^+})/hc]=\frac{\mathcal{R}_{\rm H_2}}{[\nu_{v^+N^+}(E)]^2}. \tag{9}$$

$\mathcal{R}_{\rm H_2}$ here is the mass-corrected Rydberg constant.

Line intensities are computed here for weak radiation fields as appears appropriate for astrophysical applications. The effective transition moment to the bound Rydberg state n is given by the following superposition of channel amplitudes:

$$D_n = \frac{1}{\mathcal{N}} \sum_k d_{kk''}(E_n) B_k(E_n), \tag{10}$$

where k stands for the ionization channels v^+N^+ and k'' stands for the lower state $v''N''$, respectively. $d_{kk''}(E_n)$ is the frame transformed vibronic dipole moment. $\mathcal{N}$ is the overall normalization factor of the bound-state wave functions; see Ref. [24]. It has the dimension (energy)$^{-1/2}$ which compensates the dependence (energy)$^{-1/2}$ contained in the channel moments $d_{kk''}$. The transition moment D_n for each spectral line is finally converted into an upper state emission probability according to [34]:

$$A_{n\to v''N''} = \frac{4mc^2\alpha^5}{\hbar}\left(\frac{1}{2N'+1}\right)\left(\frac{E_n - E_{v''N''}}{2\mathcal{R}hc}\right)^3 \left|\frac{D_n}{a_0}\right|^2, \tag{11}$$

where α here denotes the fine-structure constant.

In order to calculate the photoabsorption and photoionization cross sections, σ_a and σ_i, we have to consider the open ionization channels in addition to their closed counterparts. The quantization condition for an open channel j, see Eqs. (6) and (7), reads [24]

$$\sum_k [\cos(\pi\tau_\rho)\mathcal{S}_{jk} - \sin(\pi\tau_\rho)\mathcal{C}_{jk}] B_k^{(\rho)}(E) = 0, \tag{12}$$

where $\pi\tau_\rho$ is an open-channel ionization eigenphase and ρ is a solution index. In all, there are as many eigenphases as there are open channels, N_P, and there is a set of channel mixing coefficients, $B_k^{(\rho)}$, corresponding to each particular eigenphase. The total intensity is expressed in terms of a set of real dipole amplitudes which replace Eq. (10):

$$D^{(\rho)}(E) = \sum_k d_{kk''}(E) B_k^{(\rho)}(E)\ . \tag{13}$$

The apparent disagreement between Eqs. (10) and (13) reflects the different normalization of the discrete and continuum wave functions: $D^{(\rho)}(E)$ in Eq. (13) gives the dipole amplitude per unit energy and has dimension (length) × (energy)$^{-1/2}$. The total photoabsorption cross section, σ_a (equal to the photoionization cross section σ_i when no competing decay channels are present), becomes [34]

$$\sigma_a(E) = \frac{4\pi^2\alpha}{2N''+1}(E - E^+_{v^+N^+})\,[D(E)]^2\,, \tag{14}$$

where $[D(E)]^2 = \sum_{\rho=1}^{N_P} [D^{(\rho)}(E)]^2$.

C. Numerical details

The quantum defects and electronic dipole moments have been extracted from the clamped-nuclei (Born-Oppenheimer) potential energy curves and dipole moment functions of Refs. [27–29] as described in Sec. II B. The rovibrational wave functions were evaluated in the adiabatic approximation using the ion ground-state potential energy curve of Wind [30] and the adiabatic correction terms of Bishop and Wetmore [35]. The corresponding ion levels are those of Wolniewicz and Orlikowski [29], evaluated including the nonadiabatic and relativistic interactions in addition to the adiabatic corrections. These ion level energies do not include the hyperfine interactions, but their accuracy—as well as that of the potential curves and adiabatic corrections—is largely sufficient in the present context. We used for the theoretical ionization limit the value of Wolniewicz [28], i.e., 124 417.491 cm^{-1}, and the different ionization thresholds are the vibrational levels of the molecular ion. The ground-state vibrational wave function was evaluated with the potential energy curve and adiabatic corrections of Wolniewicz [29], while the ground-state rovibrational energy levels were taken from the work of Pachucki and Komasa [36]. The vibrational wave functions were integrated from $R = 0.1$ out to R_c with R_c in the range ≈10 to 12.5 a.u. Typical values of the vibrational basis were $0 \leqslant v^+ \leqslant 40$. In some cases the basis was increased up to $v^+ = 60$ in order to check the convergence. Up to $v^+ = 19$ the vibrational basis represents the 20 bound levels of the ion. For larger values v^+ it depends on the value of R_c and represents the discretized vibrational continuum.

The calculations were performed in two steps. A calculation of bound states was carried out first, in which the open channels were ignored. This provided the energies of the bound Rydberg levels and the corresponding spontaneous emission coefficients of the upper levels. In the second step the open channels were also included. The step size of the energy grid was chosen to correspond to 0.1 cm^{-1}. In the neighborhood of the bound Rydberg levels (known from the preliminary bound state calculation) the grid was chosen to correspond to 5×10^{-6} cm^{-1}, necessary in order to map out the photoabsorption (photoionization) cross section in full detail. Just below each vibrational ionization thresholds $v^+, N^+ = 1$ the Rydberg level density becomes large and we used a step size of 10^{-3} cm^{-1}. We calculated states up to $n_{\rm eff} \approx 70$, leaving an energy gap of 20 cm^{-1} below each ionization threshold.

III. RESULTS

A. MQDT calculations

The first series of calculations in which open channels were omitted yielded upper state energy levels, transition energies, wave functions, and spontaneous emission Einstein coefficients. Table I contains a selection of the strongest calculated lines ($v'' = 1$). In the second series of calculations open channels were included and Eq. (6) in its most general form was solved, providing the continuum phase shifts, channel mixing coefficients, effective transition moments, and, as the final result, the cross section for the photoabsorption process as a function of the transition energy. Figure 1(a) (upper frame) displays the corresponding continuous distribution for $v'' = 1$, while the lower frame of the same figure is organized in exactly the same way and shows the analogous distribution for $v'' = 5$. Photoabsorption eventually results in ionization and/or fluorescence and dissociation, but since at this stage the two additional decay channels dissociation and fluorescence have been neglected, the spectrum of Fig. 1(a) represents, strictly speaking, the theoretical photoabsorption spectrum, broadened by interaction with the open ionization continua. A

TABLE I. Properties of the peaks characterized as resonances connected to vibrational levels of the different electronic states lying above the ionization limit for $Q(1)$ transitions of H_2. The notation (n,v') refers to the principal and vibrational quantum numbers of the upper state, e.g., $(3,7) = 3p\pi\, D(v'=7)$. ν_n/c and $\nu(\text{obs})/c$ are the calculated and observed transition frequencies in cm^{-1}, and $[\nu_n - \nu(\text{obs})]/c$ is their difference (where available). The corresponding energies, E_n, of the upper state levels above $v''=0, N''=0$ are obtained by adding 4273.7371 cm^{-1} [36]. Γ are the calculated autoionization widths, A is the spontaneous emission probability, and $\Delta A/A$ the relative difference of the present calculation and the earlier calculations of Abgrall *et al*. [8]. A/A_{approx} is the ratio of the Einstein coefficients calculated with Eqs. (11) and (16), respectively. Horizontal gaps are indicative of the positions of the vibrational ionization thresholds $v^+, N^+ = 1$. *Threshold* stands for the closest higher vibrational level of the ion. The *relative contribution* is defined by Eq. (17).

								Ionization		Absorption	
Upper state (n,v')	ν_n/c (cm^{-1})	$[\nu_n - \nu(\text{obs})]/c$ (cm^{-1})	Γ (10^{-4} cm^{-1})	A (10^6 s^{-1})	$\Delta A/A$	A/A_{approx}	Threshold (v^+)	Relative contrib.	Total vs backgr.	Relative contrib.	Total vs backgr.
(5,2)	120 227.40		131.0	0.25		0.95		0.01		0.01	
(6,2)	121 490.07		668.8	2.48		0.86		0.13		0.05	
(3,7)	121 603.97	0.55	0.05	27.36	0.11	0.96	1	$<10^{-2}$	5.9	0.59	15.1
(4,4)	121 678.08	−0.22	1.0	0.94		0.98		0.01		0.02	
(5,3)	122 163.19		58.1	0.13		0.97		0.01		$<10^{-2}$	
(3,8)	122 974.34	−0.29	0.2	24.17	0.08	0.97		$<10^{-2}$		0.32	
(4,5)	123 387.07	−0.03	0.5	6.52		0.97		$<10^{-3}$		$<10^{-2}$	
(6,3)	123 437.68		349.8	0.22		0.97	2	0.03	1.9	$<10^{-2}$	15.9
(5,4)	123 988.41		47.7	1.26		0.97		0.13		0.02	
(3,9)	124 222.40	−0.44	0.02	20.44	0.08	0.97		0.01		0.56	
(4,6)	124 983.98		75.2	9.96		0.97		0.50		0.24	
(6,4)	125 256.71		1399.6	0.74		0.97		0.05		0.02	
(3,10)	125 347.34	−0.36	0.04	16.20	0.06	0.97	3	$<10^{-3}$	4.2	0.19	9.5
(5,5)	125 695.41		141.0	3.32		0.97		0.19		0.09	
(3,11)	126 344.18	0.09	0.2	14.89	0.2	0.97		$<10^{-2}$		0.35	
(4,7)	126 465.82		161.0	8.53		0.97		0.28		0.17	
(6,5)	126 962.52		1455.0	2.15		0.98		0.07		0.04	
(3,12)	127 210.28	0.54	0.7	10.50	0.13	0.97	4	0.01	8.1	0.19	13.5
(5,6)	127 286.68		437.5	4.59		0.97		0.16		0.10	
(4,8)	127 832.24		294.8	6.76		0.96		0.26		0.17	
(3,13)	127 937.70		0.01	6.39	−0.05	0.90		$<10^{-4}$		0.20	
(3,14)	128 517.85		5.0	5.65	0.16	0.97		0.05		0.16	
(6,6)	128 549.49		4742.2	3.89		0.98		0.12		0.08	
(5,7)	128 764.12		530.2	5.47		0.98		0.19		0.13	
(3,15)	128 945.03		0.3	3.80	0.2	0.97	5	$<10^{-2}$	7.5	0.08	11.4
(4,9)	129 084.76		25.8	7.17		0.98		0.18		0.16	
(3,16)	129 236.87		0.05	2.20	0.3	0.97		$<10^{-4}$		0.03	
(3,17)	129 518.49		0.1	2.82	0.89	0.97		$<10^{-4}$		0.06	
(6,7)	130 026.52		4673.8	5.07		0.98		0.09		0.09	
(5,8)	130 126.23		775.0	6.32		0.98		0.14		0.14	
(4,10)	130 223.83		0.3	4.27		0.93	6	0.08	12.8	0.08	12.8
(4,11)	131 227.70		0.6	7.17		0.99		0.13		0.13	
(5,9)	131 379.37		234.5	3.90		0.98		0.07		0.07	
(6,8)	131 403.42		231.3	0.10		0.98		$<10^{-2}$		$<10^{-2}$	
(4,12)	132 127.86		200.4	5.14		0.98		0.39		0.39	
(5,10)	132 519.02		456.2	3.92		0.98	7	0.09	10.7	0.09	10.7
(6,9)	132 646.95		1124.5	2.37		0.98		0.06		0.06	
(4,13)	132 900.34		15.3	3.20		0.98		0.07		0.07	
(4,14)	133 524.11		300.3	5.05		0.98		0.20		0.20	
(5,11)	133 559.46		139.2	0.02		0.97	8	$<10^{-3}$	6.2	$<10^{-3}$	6.2
(6,10)	133 784.08		2710.9	1.92		0.98		0.07		0.07	
(4,15)	134 044.90		10.7	1.58		0.98		0.07		0.07	
(4,16)	134 408.39		166.0	0.01		0.95		$<10^{-3}$		$<10^{-3}$	
(5,12)	134 449.51		1261.1	1.58		0.98		0.07		0.07	
(4,17)	134 691.00		71.0	1.03		0.97	9	0.04	6.6	0.04	6.6
(6,11)	134 811.36		2512.8	1.85		0.99		0.07		0.07	
(5,13)	135 230.90		251.7	1.58		0.98		0.06		0.06	
(6,12)	135 720.24		3038.8	1.50		0.99		0.07		0.07	
(5,14)	135 895.98		257.1	0.10		0.98	10	0.01	5.3	0.01	5.3
(5,15)	136 418.16		669.1	0.68		0.98		0.05		0.05	
(6,13)	136 511.85		1067.1	1.02		0.99		0.05		0.05	
(5,16)	136 804.28		437.0	0.70		0.98	11	0.06	4.3	0.06	4.3

logarithmic intensity scale has been used in Fig. 1(a) in order to highlight the density of autoionization structures that arise in the cross section.

The plot of Fig. 1(a) demonstrates that the cross section is dominated by the presence of resonance structures corresponding to excitation of various vibrational levels of quasibound electronic states which lie above the ionization threshold. By representing every discrete upper level by a sharp line with the intensity corresponding to its spontaneous emission probability one obtains the spectrum as a sequence of Feshbach resonances. This can be seen in Fig. 1(b). This figure and Table I only contain the lines corresponding to states up to $n = 6$, whereas the total photoabsorption cross section shown in Fig. 1(a) contains the states with higher n quantum numbers as well.

Comparison of the two frames of Fig. 1, corresponding respectively to $v'' = 1$ and $v'' = 5$, highlights the fact that while the transition moments are different for excitation from different vibrational lower levels, the resonant structures dominate the spectrum in the same way. In the following subsections we discuss in turn various aspects of the results contained in Table I and the upper frame of Fig. 1.

B. Fluorescence and dissociation processes

Once the theoretical photoabsorption spectrum has been calculated further steps are required in order to get the "true" photoionization cross section which is corrected for dissociation and fluorescence processes. To this effect we have used the data from Refs. [19,20], where absolute cross sections for the competing decay-channels fluorescence, dissociation, and ionization of photoexcited long-lived superexcited H_2 molecular levels have been reported from the ionization threshold of H_2 up to the $H(1s) + H(n = 3)$ dissociation limit. In that work total and partial natural widths of superexcited $^1\Pi_u^-$ levels have been determined experimentally and also by first-principles calculations carried out using multichannel quantum defect theory, and good agreement between experiment and theory was found. Figure 8 of Ref. [20] displays the photoionization, photodissociation, and fluorescence yields for the $3p\pi\ D$, $4p\pi\ D'$, and $5p\pi\ D''\,^1\Pi_u^-$ levels with $N = 1$, 2, and 3. These results showed that fluorescence dominates for $n = 3$ (D state) and is also present in the $n = 4$ and 5 (D' and D'' states). Photodissociation is significant ($\approx$15 to 20%) for $n = 3$, but is absent for $n = 4$ and 5. Photoionization is dominant for $n \geqslant 5$. For $n = 4$ ionization varies substantially as a function of the vibrational quantum number and of the rotational quantum number N, whereas for $n = 3$ it is a minor channel.

We proceed on the assumption that in the energy range considered here dissociation and fluorescence processes affect only the resonances but not the continuous background absorption. We further assume that the three competing decay processes are slow (typically of the order of more than a nanosecond in the resonances studied here [20]), so that the coupling between them can be neglected, no interference occurs, and consequently they are additive. It is known, as for instance has been demonstrated by the detailed model study of Watson [37] (and references therein), that partial decay widths combine additively for sharp resonances, while this is not the case for broad resonances where interference effects occur. The resonances studied here are extremely sharp as they have widths of the order of 10^{-5} or less in natural (Rydberg) units. Our procedure thus consists in renormalizing the photoabsorption cross section σ_a by multiplying each resonance profile with its corresponding photoionization yield taken from Ref. [20], and thus obtain the photoionization cross section σ_i. This is further discussed in the following Sec. III C.

C. Average cross sections

Figures 1(c) and 1(d) are designed to demonstrate the remarkable importance of resonances in the $Q(1)$ photoionization cross section. The black solid line represents the background cross section, $\sigma^{(\text{background})}(E)$, obtained when all closed channels are excluded in the calculation and hence all resonances disappear from the spectrum. This is equivalent to the approximation made, e.g., in the earlier Refs. [11,12]. The background cross section increases by a step at each vibrational threshold, whereby each step height is approximately proportional to the Franck-Condon factor $\langle v^+|v''\rangle^2$ between the initial vibrational state and the newly opened channel v^+. The vibrational thresholds are marked by dotted vertical lines in Fig. 1. Notice how these steps do not stand out at all in the full photoabsorption spectrum shown in Fig. 1(a).

In order to assess the importance of the resonances we have for each vibrational interval calculated the averaged photoabsorption and photoionization cross sections according to

$$\bar{\sigma}_a(v^+) = \frac{\int_{E_{v^+}}^{E_{v^+ +1}} \sigma_a(E) dE}{E_{v^+ +1} - E_{v^+}}. \tag{15}$$

The averaged photoionization cross section, $\bar{\sigma}_i(v^+)$, and background cross sections, $\bar{\sigma}_i^{(\text{background})}(v^+) = \bar{\sigma}_a^{(\text{background})}(v^+)$, were evaluated in an analogous manner. Note that the dependence of the averages on the ionization thresholds shows that the averaging was done between two consecutive thresholds [dotted vertical lines in Figs. 1(c) and 1(d), respectively]. The averaged cross sections $\bar{\sigma}_a$ and $\bar{\sigma}_i$ are indicated in Figs. 1(c) and 1(d) by dashed horizontal lines (red online), respectively.

We found that at lower photon energies, near threshold, the resonance enhancement exceeds the background cross section by more than one order of magnitude, while at higher energies it is still more than a factor of 2 larger than the latter. Table I lists for each ion core vibrational interval $(v^+, v^+ + 1)$ the quantity $\bar{\sigma}_{i \text{ or } a} \,/\, \bar{\sigma}_{i \text{ or } a}^{(\text{background})}$ giving the ratio of the total versus the background (*total vs backgr.*) for ionization (i) and for absorption (a).

D. Characteristics of individual resonances

Table I lists the characteristics of the vibronic Rydberg levels $(n, v') = np\pi\ ^1\Pi_u^-, v', N' = 1$ with $n = 3$–6 that lie above the ionization threshold and are excited via $Q(1)$ transitions from $X\ ^1\Sigma_g^+(v'' = 1)$. In the table are listed the calculated transition frequencies ν_n/c and widths Γ (full width at half maximum) for each level. The transitions are referred to the ground-state level $v'' = 1, N'' = 1$ which lies 4273.7371 cm^{-1} above the ground level [36]. The table further lists the deviations of the differences between the observed and calculated frequencies, $[\nu_n - \nu(\text{obs})]/c$, as well as the relative

differences, where available, of the spontaneous emission probabilities obtained here for each upper level and the earlier calculation of Abgrall *et al.* [8], which have been derived without any coupling. The positions and autoionization widths have been determined for each resonance from the resonance profile and phase shift sum.

As a check of the correctness of the MQDT calculations the Einstein A coefficient may also be extracted for each resonance from the calculated integrated cross section. Assuming a Lorentzian resonance shape one finds that the Einstein coefficient is related to the integrated cross section as follows [38]:

$$A_{\rm approx} \approx 4\pi^2 c \left(\frac{2N'+1}{2N''+1}\right)\left(\frac{E_n - E_{v''N''}}{hc}\right)^2 \left(\frac{\Gamma}{hc}\right)\sigma_{\rm max}, \tag{16}$$

with $\sigma_{\rm max}$ the peak value of the resonance profile and Γ its width. Recall that for Q transitions $N' = N''$. The ratios $A/A_{\rm approx}$ of the two Einstein coefficients are given in Table I. It may be seen that the two ways of calculating the A coefficients agree to within less than 10%. The values derived from Eq. (16), however, are systematically a few percent larger than those obtained with Eq. (11), no doubt because the profile asymmetry (Fano q parameter) has not been taken into account in the expression (16).

Table I also lists the relative contributions, R_i and R_a, of each of the listed resonances to the total photoionization or photoabsorption, respectively, in the corresponding vibrational interval, viz.

$$R_{i\ {\rm or}\ a} = \frac{\int_{E_0-\epsilon}^{E_0+\epsilon} \sigma_{i\ {\rm or}\ a}(E)dE}{\int_{E_{v^+}}^{E_{v^++1}} \sigma_{i\ {\rm or}\ a}(E)dE}. \tag{17}$$

The integration range 2ϵ around each resonance was chosen large enough, $\epsilon \simeq m\Gamma$, $m > 10$, such as to contain the bulk of the resonance.

IV. DISCUSSION

One of the interesting features emerging from our calculations—which confirms the findings of the earlier Refs. [19,20]—is the fact that the resonances associated with the $3p\pi\ D$ Rydberg state—the electronically least excited state present in the energy range studied here—are characterized by the smallest widths. This is borne out by the results listed in Table I, and, indeed, is the reason why dissociation and fluorescence are able to compete with autoionization in the $3p\pi\ D$ state levels. As n increases, the widths initially increase also, and the broadest resonances which we have encountered are associated with the $6p\pi\ D'''$ state. Levels with higher n again have smaller widths. This at first sight surprising behavior may be traced back to the double dependence on n and v of the nonadiabatic discrete-continuum interactions. The (squared) electronic Rydberg-state–continuum coupling has an overall dependence proportional to n^{*-3}, whereas the interconversion of electronic and vibrational energy is favored when the difference $v^+ - v'$ is small [cf. Eq. (4)]. The low-n states have the highest v' values among the resonances anywhere above the ionization potential, so that their coupling to the continua is weak despite their low electronic excitation. The two opposing tendencies produce the trends visible in Table I.

TABLE II. Relative contributions of the resonances associated with the $n = 3$–6 electronic states to the photoabsorption and photoionization cross sections for H_2, $v'' = 1$, and $Q(1)$ transitions.

		Ionization		Absorption	
Upper state	Number of resonances	Overall contrib.	Total vs backgr.	Overall contrib.	Total vs backgr.
$3p\pi\ D$	11	0.01		0.16	
$4p\pi\ D'$	14	0.23	6.2	0.10	8.1
$5p\pi\ D''$	15	0.12		0.06	
$6p\pi\ D'''$	12	0.08		0.04	

Our calculations further indicate that the $3p\pi\ D$ levels contribute most strongly to the photoabsorption cross section, whereas the $4p\pi\ D'$ levels are the most prominent contributors to the photoionization cross sections. Indeed, in some energy intervals the $n = 3$ and 4 levels produce nearly the totality of the predicted photoabsorption and photoionization cross section. For instance, in the energy range between the $v^+ = 1$ and $v^+ = 2$ thresholds the contribution of the two $3p\pi\ D$ levels with $v' = 8$ and 9 accounts for almost 90% of the photoabsorption cross section (see Table I). Table II gives the overall contribution of the vibrational levels of the lowest four excited electronic states, $n = 3$–6, compared to the total photoionization and/or photoabsorption cross section. Thus, while Table I compares the total and background cross sections in the ranges between consecutive ionization thresholds, we have summed up in Table II the contributions of individual electronic states over the whole interval under study. It turns out that more than 42% of the total photoionization cross section and more than 35% of the photoabsorption cross section are produced by the four lowest electronic states. We conclude the discussion by pointing to the fact that once the excitation energy exceeds the $H(1s) + H$ ($n = 3$) dissociation limit [indicated by a vertical full line (blue online); cf. Figs. 1(c) and 1(d)], the absorption and ionization cross sections become equal and eventually tend toward the background cross section.

V. CONCLUSION

This paper is the first of a series intended to provide theoretical data concerning photoabsorption and photoionization from vibrationally excited diatomic hydrogen, H_2. We believe that our MQDT approach is reliable as it has been tested previously by extensive comparison with experimental results concerning photoexcitation from the vibrational ground state of the molecule [18–20]. One might argue that a weakness of our approach is that we have used clamped-nuclei transition moments evaluated [29] for excitation to relatively low electronically bound states ($n = 3$–5) that do not pertain to the continuum. Indeed, we have used MQDT methodology to determine the energy dependence of the corresponding energy-normalized channel transition moments (Sec. II B), and we hence extrapolated to the electronic continuum. On the other hand, it appears that the possible error associated with this extrapolation must be largely compensated by the fact that the photoionization cross section is dominated by quasibound

autoionization resonances and not by the electronic continuum itself; in other words, the resonances—the calculated intensities of which are known to be highly accurate—carry far more intensity than the structureless background.

We finally wish to emphasize the possible relevance of the present work for the physics of the interstellar medium. For excitation of ground state H_2 from $v'' = 5$, the Lyman limit lies higher than the $v^+ = 0$ and 1 ionization thresholds as shown by the lower frame of Fig. 1, so that the resonance phenomena which have been the subject of this paper should become fully effective.

ACKNOWLEDGMENTS

The authors acknowledge support from the French Agence Nationale pour la Recherche under Contract No. 09-BLAN-02090 "SUMOSTAI." Ch.J. thanks the Miescher Foundation (Basel, Switzerland) for partial support. Ch.J., J.Zs.M., and I.F.S. acknowledge support from the International Atomic Energy Agency (CRP "Light Element Atom, Molecule and Radical Behaviour in the Divertor and Edge Plasma Regions" and "Atomic and Molecular Data for State-Resolved Modelling of Hydrogen and Helium and Their Isotopes in Fusion Plasma"). I.F.S. and J.Zs.M. are grateful to the "Triangle de la Physique" Palaiseau-Orsay-Saclay (France) and the Conseil Régional de la Haute Normandie for their support. Finally, I.F.S. acknowledges help from the European Spatial Agency (ESTEC 21790/08/NL/HE), the French Research Federation for Fusion Studies, the CNRS/INSU programme PCMI, and the IEFE institute Rouen-Le Havre, and he is grateful for the hospitality of the Laboratoire Aimé Cotton extended to him during this work.

[1] P. F. Goldsmith, T. Velusamy, D. Li, and W. D. Langer, Astrophys. J. **715**, 1370 (2010).
[2] F. Le Petit, C. Nehmé, J. Le Bourlot, and E. Roueff, Astrophys. J. Suppl. Ser. **164**, 506 (2006).
[3] Y. Sheffer, J. X. Prochaska, B. T. Draine, D. A. Perley, and J. S. Bloom, Astrophys. J. **701**, L63 (2009).
[4] D. M. Meyer, J. T. Lauroesch, U. Sofia, B. T. Draine, and F. Bertoldi, Astrophys. J. **553**, L59 (2001).
[5] P. Gnacinski, Astron. Astrophys. **532**, 122 (2011).
[6] http://molat.obspm.fr/index.php?page=pages/Molecules/H2/H2can94.php.
[7] H. Abgrall, E. Roueff, F. Launay, J. Y. Roncin, and J. L. J. Subtil, J. Mol. Spectrosc. **157**, 512 (1993).
[8] H. Abgrall, E. Roueff, F. Launay, and J. Y. Roncin, Can. J. Phys. **72**, 856 (1994).
[9] H. Abgrall, E. Roueff, F. Launay, J. Y. Roncin, and J. L. J. Subtil, Astron. Astrophys. Suppl. Ser. **101**, 273 (1993).
[10] H. Abgrall, E. Roueff, F. Launay, J. Y. Roncin, and J. L. J. Subtil, Astron. Astrophys. Suppl. Ser. **101**, 323 (1993).
[11] A. L. Ford, K. K. Docken, and A. Dalgarno, Astrophys. J. **195**, 819 (1975).
[12] A. L. Ford, K. K. Docken, and A. Dalgarno, Astrophys. J. **200**, 788 (1975).
[13] M. R. Flannery, H. Tai, and D. L. Albritton, At. Data Nucl. Data Tables **20**, 563 (1977).
[14] S. V. O'Neil and W. P. Reinhardt, J. Chem. Phys. **69**, 2126 (1978).
[15] C. M. Coppola, S. Longo, M. Capitelli, F. Palla, and D. Galli, Astrophys. J. Suppl. Ser. **193**, 7 (2011).
[16] J. Zs. Mezei, I. F. Schneider, and Ch. Jungen (in preparation).
[17] M. Glass-Maujean, S. Klumpp, L. Werner, A. Ehresmann, and H. Schmoranzer, Mol. Phys. **105**, 1535 (2007).
[18] M. Glass-Maujean and Ch. Jungen, J. Phys. Chem. **113**, 13124 (2009).
[19] M. Glass-Maujean, Ch. Jungen, H. Schmoranzer, A. Knie, I. Haar, R. Hentges, W. Kielich, K. Jänkälä, and A. Ehresmann, Phys. Rev. Lett. **104**, 183002 (2010).
[20] M. Glass-Maujean, Ch. Jungen, G. Reichardt, A. Balzer, H. Schmoranzer, A. Ehresmann, I. Haar, and P. Reiss, Phys. Rev. A **82**, 062511 (2010).
[21] G. D. Dickenson, T. I. Ivanov, M. Roudjane, N. de Oliveira, D. Joyeux, L. Nahon, W.-Ü. L. Tchang-Brillet, M. Glass-Maujean, I. Haas, A. Ehresmann, and W. Ubachs, J. Chem. Phys. **133**, 144317 (2010).
[22] C. H. Greene and Ch. Jungen, Adv. At. Mol. Phys. **21**, 51 (1985).
[23] *Molecular Applications of Quantum Defect Theory*, edited by Ch. Jungen (The Institute of Physics, Bristol and Philadelphia, 1996).
[24] Ch. Jungen, in *Elements of Quantum Defect Theory*, Handbook of High-resolution Spectroscopy, edited by M. Quack and F. Merkt (Wiley & Sons, New York, 2011), p. 471.
[25] Ch. Jungen, I. Dabrowski, G. Herzberg, and D. J. W. Kendall, J. Chem. Phys. **91**, 3926 (1989).
[26] Ch. Jungen, S. T. Pratt, and S. C. Ross, J. Phys. Chem. **99**, 1700 (1995).
[27] L. Wolniewicz and G. Staszewska, J. Mol. Spectrosc. **220**, 45 (2003).
[28] L. Wolniewicz, J. Chem. Phys. **103**, 1792 (1995).
[29] A compilation of the numerical data published in Refs. [27,28] can be found in http://hel.fizyka.umk.pl/ftp/pub/publications/ifiz/luwo/.
[30] H. Wind, J. Chem. Phys. **42**, 2371 (1965).
[31] G. W. F. Drake, in *High Precision Calculations for Helium*, Springer Handbook of Atomic, Molecular, and Optical Physics, edited by G. W. F. Drake (Springer, New York, 2006), p. 199.
[32] N. Y. Du and C. H. Greene, J. Chem. Phys. **85**, 5430 (1986).
[33] S. C. Ross and Ch. Jungen, Phys. Rev. A **49**, 4364 (1994).
[34] M. Glass-Maujean, Ch. Jungen, H. Schmoranzer, I. Haar, A. Knie, P. Reiss, and A. Ehresmann, J. Chem. Phys. **135**, 144302 (2011).
[35] D. M. Bishop and R. W. Wetmore, Mol. Phys. **26**, 145 (1973); **27**, 279 (1974).
[36] K. Pachucki and J. Komasa, J. Chem. Phys. **130**, 164113 (2009).
[37] D. K. Watson, J. Phys. B **19**, 293 (1986).
[38] R. C. Hilborn, Am. J. Phys. **50**, 982 (1982).